This manuscript has been published online in: Acta Biomaterialia May 2019

https://doi.org/10.1016/j.actbio.2020.05.002

Title: Polymeric nanoparticles protect the resin-dentin bonded interface from cariogenic biofilm degradation.

Running title: Nanoparticles antidegradation activity at bonded dentin.

Authors:

Manuel Toledano-Osorio[a], Raquel Osorio[a], Fátima S Aguilera[a], Antonio Luis Medina-Castillo[b], Manuel Toledano[a*], Estrella Osorio[a], Sergio Acosta[c], Ruoqiong Chen[d], Conrado Aparicio[e].

Institution:

[a] University of Granada, Faculty of Dentistry, Dental Materials Section.
Colegio Máximo de Cartuja s/n
18071 – Granada - Spain.

[b] University of Granada, NanoMyP. Spin-Off Enterprise.
Edificio BIC-Granada. Av. Innovación 1.
18016 - Armilla, Granada, Spain.

[c] Bioforge lab, CIBER-BBN, Edificio LUCIA, University of Valladolid, Paseo Belen 19, Valladolid 47011, Spain.

[d] Department of Diagnostic and Biological Sciences, School of Dentistry, University of Minnesota, Minneapolis, MN, USA.

[e] MDRCBB-Minnesota Dental Research Center for Biomaterials and Biomechanics, Department of Restorative Sciences, School of Dentistry, University of Minnesota, Minneapolis, MN, USA.

*Corresponding author: Prof. Manuel Toledano.
University of Granada, Faculty of Dentistry
Dental Materials Section
Colegio Máximo de Cartuja s/n
18071 – Granada - Spain.
Tel.: +34-958243788
Fax: +34-958240809

ABSTRACT

The objective was to assess doxycycline (Dox) and zinc (Zn) doped nanoparticles' (NPs) potential to protect the resin-dentin interface from cariogenic biofilm. Three groups of polymeric NPs were tested: unloaded, loaded with zinc and with doxycycline. NPs were applied after dentin etching. The disks were exposed to a cariogenic biofilm challenge in a Drip-Flow Reactor during 72 h and 7 d. Half of the specimens were not subjected to biofilm formation but stored 72 h and 7 d. LIVE/DEAD® viability assay, nano-dynamic mechanical assessment, Raman spectroscopy and field emission electron microscopy (FESEM) analysis were performed. The measured bacterial death rates, at 7 d were 46% for the control group, 51% for the undoped-NPs, 32% for Dox-NPs, and 87% for Zn-NPs; being total detected bacteria reduced five times in the Dox-NPs group. Zn-NPs treated samples reached, in general, the highest complex modulus values at the resin-dentin interface over time. Regarding the mineral content, Zn-NPs-treated dentin interfaces showed the highest mineralization degree associated to the phosphate peak and the relative mineral concentration. FESEM images after Zn-NPs application permitted to observe remineralization of the etched and non-resin infiltrated collagen layer, and bacteria were scarcely encountered. The combined antibacterial and remineralizing effects, when Zn-NPs were applied, reduced biofilm formation. Dox-NPs exerted an antibacterial role but did not remineralize the bonded interface. Undoped-NPs did not improve the properties of the interfaces. Application of Zn-doped NPs during the bonding procedure is encouraged.

Keywords: dentin, degradation, interface, nanoparticle, biofilm

1. Introduction

In dentistry, restorations based on adhesive resins are widespread due to the aesthetic properties and the handling characteristics of these materials. But adhesive restorations have a high failure rate. After 8 years, composite restorations had at least 50% greater failure percentage and 3.5 times higher secondary decay incidence than amalgam [1]. The adhesive bond layer integrity of composite restoration, *i.e*, the quality of the interface between the tooth and the restoration, is the most important factor that determines the long-term success of restorations [1–4].

In clinical dentistry, the most frequently involved substrate for adhesion is dentin [5]. The structure of dentin is comprised of around 50 vol% mineral. This mineral is present in the form of apatite crystallites, characterized by a carbonate enrichment and calcium deficiency. It is distributed between dentinal tubules which run parallel. The other 50 vol% is water, collagen and other minor non-collagenous proteins [6]. Dentin adhesion is promoted when the substrate's mineral phase is removed by acids and the voids formed by mineral are filled with adhesive resin, which is subjected to an *in situ* polymerization, creating the hybrid layer (HL) [7]. Collagen is not easily penetrated by resins, after acid etching. Differential dentin diffusion depth between acids and resins produces a demineralized/non-resin infiltrated collagen layer, located right at the bottom, and named bottom of the hybrid layer (BHL). It is considered an interfacial microgap and the weak link at the composite restorations [1]. The BHL is susceptible to degradation by intrinsic host-derived matrix metalloproteinases (MMPs) or bacterial activity [8].

Bacterial microleakage is the most common complication among composite restorations, and secondary caries is the principal failure cause [2,3,9]. Biofilm formation at the restoration-tooth interface [10] is probably assisted by the gap formed between both structures that enables the colonization of bacteria [11], thereby facilitating secondary caries [3,12,13]. The pH decrease caused by bacteria acid production, alters the equilibrium and dissolves hydroxylapatite, leading to further dentin demineralization [14–16]. Then, the existing gaps at the resin-dentin bond in junction with an increase in levels of bacteria at the perimeter of

composite materials leads to a key relationship between microbiology and adhesive degradation as crucial elements in the failure of these adhesive restorations [1,17,18]. Bacteria cannot be eliminated from the oral environment, and they have been shown to form a micro-ecosystem known as a biofilm [1]. The reduction of the pathogenic impact of the biofilm at the margin of the composite restoration by engineering anti-cariogenic materials is desired [1,17–19].

Biocompatible and non-reabsorbable polymeric nanoparticles (NPs), comprised of methacrylic acid, ethylene glycol dimethacrylate and 2-hydroxyethyl methacrylate covalently connected [20], has been proposed to hinder the formation of secondary caries and extend adhesive restorations longevity [21]. Antibacterial and remineralizing agents can be chemically attached to the polymer carrier through functional carboxyl groups that are along the surface of the NPs [9,22]. Doxycycline and zinc have been previously doped onto these NPs and an antibacterial [23] and antibiofilm formation effects were demonstrated on hydroxyapatite discs [24]. Furthemore, NPs were previously employed at the resin-dentin bonded interface, and it was stated that they do not interfere the bonding process and also may produce collagen protection from dentin MMPs [22,25].

The objective of this research was to assess the doxycycline and zinc loaded-NPs potential to protect the resin dentin interface from a cariogenic biofilm.

Measuring the effects of antibacterial agents at the bonded interface in a simulated oral environment is challenging. A multifactorial deleterious effect of bacteria at the bonded interface has been reported [26]. A LIVE/DEAD® staining technique contributes to determine the presence and growth of the biofilm at the resin-dentin interface [17]. Bacterial localization may also be qualitatively analyzed by scanning electron microscopy. Nano-DMA represents a crucial tool to detect the bonded interface degradation trough reduction in mechanical properties of the bonded interface that primary resulted from dentin demineralization [27]. High biochemical specificity analysis of the resin-dentin interface through complementary Raman spectroscopy has also been proposed [28].

The null hypothesis to be tested is that infiltration of doxycycline and zinc loaded-NPs into etched dentin, previous to the resin application step, does not exert protection of the hybrid

layer from the *in vitro* degradation activity of a cariogenic biofilm.

2. Materials and methods

2.1. Nanoparticles fabrication and loading

PolymP-*n* Active nanoparticles were used (NanoMyP®, Granada, Spain). These particles are synthetized following a polymerization precipitation procedure. NPs are composed by a main monomer, 2-hydroxyethyl methacrylate, a cross-linker, ethylene glycol dimethacrylate, and a functional monomer, methacrylic acid. Detailed description of NPs composition and production is available [20]. NPs zinc-doping is obtained via immersion of 25 mg of NPs in 25 ml aqueous solutions of $ZnCl_2$ (40 mgL^{-1}), or in 25 ml of doxycycline hyclate aqueous solution (Sigma Aldrich, ChemieGmbh, Riedstr, Germany) at 750 mgL^{-1}, during 30 min under constant shaking for 20 and 90 min respectively. Suspensions were then subjected to a centrifugation process for 20 min (7,800 rpm/G-force=6,461) and the particles washed in phosphate buffered solution (PBS) and detached from the supernatant [25,29]. The attained absorption equilibrium of zinc as a time function and $ZnCl_2$ solution concentrations was previously assessed [30] and the maximum attained zinc complexation value (2 µg Zn/mg NPs) was used to load NPs in the present study. Doxycycline doping values for NPs as a function of incubation time and doxycycline concentrations was also measured [30] and the maximum doxycycline adsorption value of 27.1 µg Dox/mg NPs was selected to load NPs for the present research. It has been previously shown that the size of NPs does not change after loading, and no agglomeration is produced. Hydrodynamic size distribution of nanoparticles is NPs 250.1 ± 7.5 nm, Dox-NPs 244.4 ± 9.8 nm and Zn-NPs 225.9 ± 8.9 nm [31].

2.2. Multispecies biofilm stocks

Frozen (-80ºC) multispecies biofilm stocks from multiple subjects were used. Plaque was collected from dental restorations margins [32]. University of Minnesota Institutional Review Board approved the original human plaque sampling protocol used to prepare the stocks. Employed stocks from microcosm biofilms were representative of the oral microbiota. Biofilm validation and a complete biofilm characterization may be found in Rudney et al., [33].

2.3. Dentin disks preparation

The dentin disks preparation was made following Li et al., 2014 [18]. Disk specimens were made using bovine incisors. The bovine teeth were stored in 1.0% Chloramine T solution. The media was replaced once a week by freshly prepared solutions and stored in 4◦C before use. The crowns were cut off at the cement-enamel junction (CEJ) with a low-speed diamond saw (Isomet, Buehler, LakeBluff, IL, USA) under cooling water to provide the root dentin portion. These specimens were then trimmed down into dentin cylinders of 5 mm in diameter (concentric and parallel with the enlarged root canals), and the root canals were enlarged to 2 mm in diameter using Gates–Glidden drills. The cylinders were transversely cut to produce round disks of about 4 mm. After this process, they were rinsed 3 times with distilled water, stored in 1.0% Chloramine T solution for 7 days at 4◦C before being used. A total of 88 disks were prepared.

2.4. Dentin-composite disks fabrication

The disks were then rinsed in distilled water and dried out. To proceed with the composite filling, a common adhesion protocol was followed. The inner surface of the disks was subjected to an etching process with 35% phosphoric acid during 20 s. The disks were subsequently rinsed with distilled water and slightly dry. Disks were randomly divided into four groups (n=22), regarding NPs application: 1) NPs were not applied (ethanol was used instead of the NPs suspension); 2) undoped NPs; 3) Dox-NPs; and 4) Zn-NPs. The different NPs in ethanol suspensions (10 mg/ml) were then applied on the etched surfaces of the disks before the adhesive application. Single Bond (SB) (3 M ESPE, St. Paul, MN, USA) adhesive, was placed to the inner surface and polymerized, following manufacturer's instructions. The disks were completely filled with Z-100^{TM} (3 M ESPE, St. Paul, MN, USA), which was applied incrementally and light cured for 40 s. The two surfaces of the disks were then ground flat (180-grit) (Figure 1).

2.5. In vitro biofilm challenging model

Sixteen samples from each group were randomly selected (n=64). Before being exposed to biofilm, the bottom and the side surfaces of disks were covered with acid resistant nail

varnish. From the upper surface, only the outer part of the disk was nail varnished (leaving unprotected the resin-dentin interface and the resin surface). Samples were immersed for 5 min in 75% ethanol, air-dried and sterilized under UV light for 20 minutes [32]. The following steps were performed inside the high efficiency particulate air (HEPA) enclosure. The unprotected *(not covered with nail varnish) resin-dentin interface and resin* surfaces were coated with 10µl filter sterilized whole saliva for 5 minutes. 10µl of multispecies biofilm solution (769NS) from a 1:100 dilution of the bacterial stock were inoculated on the top of the saliva coating for another 5 minutes. Disks where then placed in a well plate (one disk per well) and covered with 1.5 ml of sterile basal mucin medium (BMM) and incubated at 37°C, 5% CO_2 for 24 h. After this period, the samples were transferred into a 4 channel Drip-Flow Reactor with a 37ºC incubator with a pump rate of 0.28 ml/minute. Two time points were established for analyzing the biofilm samples: 72 h (24 h of plate + 48 h of reactor) and 1 week (24 h of plate + 6 d of reactor). Half of the samples (n=32) were subjected to each time point. The other twenty-four samples, 3 from each group were incubated following the same procedure but without bacteria inoculation. After getting them out of the reactor different treatments were carried out depending on the analyzing method.

2.6. LIVE/DEAD® viability assay

Three disks per each group, from those subjected to bacteria challenge, were gently submerged into 0.9% NaCl to remove the unattached bacteria. For cell viability assessment, the fluorescent stains solution was prepared (L7012, LIVE/DEAD® BacLight Bacterial Viability Kit, ThermoFisher Scientific, Waltham, MA, USA) by adding 3 µl of SYTO9 green stain and 3 µl of Propidium iodide red stain to 1 ml of sterilized Milli-Q ultrapure water. 100 µl of staining solution was added. After 20-30 min in light-protected incubation at room temperature, the *biofilms grown on top the unprotected areas of the* disks were analyzed by confocal laser scanning microscopy (CLSM) with a multiphoton confocal microscope (A1R-HD, Nikon Instruments Inc., Japan). A 25x water immersion objective (Apo LWD, 1.1 NA) was used to directly visualize the biofilms. Fluorescence emissions were collected at 488 nm for Syto9 (living cells) and at 561 nm for propidium iodide (dead cells). 512 x 512 and 1024 x 1024 pixel

areas were scanned, and the Z-stacks were recorded every 0.375 µm. Images were analyzed using an image analysis software (ImageJ B, National Institutes of Health, Bethesda, Maryland, USA), by measuring voxel intensities from two-channel images, and therefore calculating the cell viability percentage within the stacks. Substraction of the background signal was performed.

2.7. Nanodynamic mechanical (NanoDMA) assessment

Three different disks from each group were subjected to nanoDMA. Disks were slightly polished (2400 to 4000 grit and 1 µm diamond paste) and thoroughly washed with deionized water. Property mappings were realized using a Ti-750D TriboIndenter (Hysitron, Inc., Minneapolis, MN) equipped with nano-DMA III, a commercial nano-DMA package. The nanoindenter tip was calibrated against a fused quartz sample using a quasistatic force setpoint of 5 µN to maintain contact between the tip and the sample surface. A dynamic (oscillatory) force of 5 µN was superimposed on the quasistatic signal at a frequency of 200 Hz. Based on a calibration modulus of the tip value of 1.1400E+3 N/mm2 for the fused quartz, the best-fit spherical radius approximation for tip was found to be 150 nm, for the selected nano-DMA scanning parameters. Modulus mapping of our samples was conducted by imposing a quasistatic force setpoint, Fq =5 µN, to which we superimposed a sinusoidal force of amplitude FA=1.8 µN and frequency f=200 Hz. Data from regions approximately 20×20 µm in size were collected using a scan rate of 0.2 Hz. Each scan resulted in a 256×256 pixel data array. Specimens were scanned in the hydrated condition. Regions of interest for analysis were selected just below the adhesive layer. Under steady conditions (application of a quasistatic force) the indentation modulus of the tested sample, E, was obtained by application of different models that relate the indentation force, F, and depth, D [34]. Data from the hybrid layer (HL), bottom of hybrid layer (BHL) were acquired, as represented in the Fig. 1.

2.8. Raman spectroscopy

The same dentin surfaces mentioned above were subsequently studied by Raman spectroscopy. For this analysis, a dispersive Raman spectrometer/microscope (Horiba Scientific Xplora, Villeneuve d´Ascq, France) with a 785-nm diode laser through a X100/0.90 NA air

objective was employed. A 600-lines/mm grafting was used to obtain Raman signals. The surfaces were subjected to a chemical mapping. Two surface areas of 20x20 μm were mapped at dissimilar sites for each sample at X and Y axis with a 0.5 μm spacing (625 points per map). Regions of interest for analysis were selected just below the adhesive layer. A cluster algorithm represents a statistical description of the cluster centroids grouped by their components. Biochemical content in each cluster was examined through the average cluster spectra. A multivariate analysis was performed using the hierarchical clustering analysis. The output from a clustering algorithm was basically a statistical description of the cluster centroids with the number of components in each cluster. Thus, chemical mapping was submitted to K-means cluster (KMC) analysis using the multivariate analysis tool (ISys® Horiba), which includes statistical pattern to derive the independent clusters. The natural groups of components (or data) based on some similarity and the centroids of a group of data sets were found by the clustering algorithm once calculated by the software and the Hierarchical Cluster Analysis (HCA). To determine cluster membership, this algorithm evaluated the distance between a point and the cluster centroids based on the Ward's Method. The observed spectra were described at 400-1700 cm^{-1} with 10 complete overlapping Gaussian lines, suggesting homogeneous data for further calculations [35]. Baseline correction and normalization on the CH_2 band 1452 cm^{-1} were performed. At this point, the components of the dentin mineral were assessed as the relative presence of mineral analysis referred to phosphate (960 cm^{-1}) peak, and the relative mineral concentration of phosphate (PO_4^{3-}) referred to phenyl (RMC: ratio between mineral [960 cm^{1}]/Phenyl [1003 cm^{-1}]). Additional peaks were measured at 1023, 1043 and 1052 and 1072 which increased in the caries spectrum [36]. The intensity ratio plot of 579/959, 590/959, were also measured to determine the presence of carious lesion [37]. Dentin organic component was analyzed examining the collagen at 937 cm^{-1} bands [38], AGEs (advance glycation end products)-pentosidine at 1550 cm^{-1}, interpreted as a marker of the aging process [39], and the ratio 1674 (amide I)/1690-1701cm^{-1} interpreted as a collagen quality parameter [40].

2.9. Field Emission Electron Microscopy (FESEM) analysis

Two specimens, of those groups subjected to bacterial challenge, were fixed for 24 h in a 2.5% glutaraldehyde solution in 0.1 mol/L sodium cacodylate buffer, rinsed three times in 0.1 mol/L sodium cacodylate buffer. Samples were placed in an apparatus for critical point drying (Leica EM CPD 300, Wien, Austria). They were then sputter-coated with carbon by means of a sputter-coating Nanotech Polaron-SEMPRE2 (Polaron Equipment Ltd., Watford, UK) and observed with a field emission scanning electron microscope (FESEM Gemini, Carl Zeiss, Oberkochen, Germany) at an accelerating voltage of 2.5 to 3 kV.

2.10. Statistical Methods

Normal distribution of data was probed by Kolmogorov-Smirnov test ($p>0.05$). Descriptive statistics for quantitative variables provides arithmetic mean as a measure of central tendency of data sets and standard deviation as a dispersion measurement. Margin of error was determined at a 95% confidence level. Sample size was standardized from previous experimental data. Statistical analysis was performed with multiple ANOVA, including interactions analysis. Student-Newman-Keuls multiple comparisons tests were employed to compare groups with different NPs ($P<0.05$). Comparisons between storage times and bacterial challenge within the same NPs groups were performed with Student t test ($P<0.01$). Normal distribution of data was probed by Kolmogorov-Smirnov test ($p>0.05$). Descriptive statistics for quantitative variables provides arithmetic mean as a measure of central tendency of data sets and standard deviation as a dispersion measurement. Margin of error was determined at a 95% confidence level. Sample size was standardized from previous experimental data. Statistical analysis was performed with multiple ANOVA, including interactions analysis. Student-Newman-Keuls multiple comparisons tests were employed to compare groups with different NPs ($P<0.05$). Comparisons between storage times and bacterial challenge within the same NPs groups were performed with Student t test ($P<0.01$).

3. Results

3.1. LIVE/DEAD® viability assay

The LIVE/DEAD® assay and fluorescent confocal laser scanning microscopy (CLSM) post-test evaluation confirmed, at each sample interface, the existence of biofilm containing live and injured or dead bacteria. An example cross section schema of the dentin bonded interface is shown in Fig. 1. After 72 h and 7 d of development, CLSM analysis demonstrated the existence of biofilms with different structures depending on the applied NPs (Fig. 1SI). The highest dead/damaged cells percentage was observed at the resin-dentin interfaces biofilm treated with Dox-NPs after 72 h and Zn-NPs after 7 d (80% and 87 % respectively). After 7d, bacterial growth (total counts -mean $\pm$ standard deviations in pixels-) was similar for all tested groups (being for the controls 3930$\pm$1534, 3758$\pm$1113 for undoped-NPs and 2406$\pm$1369 for Zn-NPs) except for the Dox-NPs groups in which total bacterial counts were reduced about five times (680$\pm$787). The measured dead/injured cells rates after 7 d were 46% for the control group, 51% for the undoped-NPs, 32% for Dox-NPs, and 87% for Zn-NPs (Table 1; Fig. 1SI).

3.2. Nanodynamic mechanical (NanoDMA) assessment

After 7 d time point, Zn-NPs-treated samples displayed the highest storage modulus (*E'*) values among groups with biofilm challenge at both the HL and BHL. Specimens treated with Zn-NPs and exposed to biofilm showed higher *E´* than samples treated with Dox-NPs, at 7 d of challenge. (Table 1SI). Undoped NPs-treated specimens and controls showed the highest and lowest loss modulus (*E''*), respectively, at both the HL and BHL with biofilm challenge after 7 d of storage. Zn-NPs treated and control samples decreased their *E''*, at the HL over time, when exposed to biofilm. Only control specimens reduced their *E''* at the BHL over time with biofilm challenge (Table 1SI).

Among groups, Zn-NPs treated specimens reached the highest complex modulus values (*E**) at the HL, regardless the storage time and the presence of biofilm. When the biofilm was absent. At 7 d time point, the rest of the groups performed similarly. Biofilm challenge produced lower *E** in the control and in the undoped-NPs groups, at both HL and BHL (Fig. 2). In the biofilm challenged group, specimens treated with both Dox-NPs and Zn-NPs achieved the highest *E** at the BHL at 7 d of storage (Fig. 2). At the HL of specimens without biofilm, *E**

increased over time when undoped-NPs and Dox-NPs were applied, while control and Zn-NPs treated samples did not change their *E** after 7 d of storage. Exposure to biofilm promoted a significant decline of *E** when controls and undoped-NPs were used, over time. Dox-NPs and Zn-NPs did not modify their resistance to deformation after 7 d of storage (Fig. 2). At the BHL of specimens without biofilm, *E** increased over time in all groups except when Zn-NPs were applied which showed similar values at both time points (72 h *vs* 7 d). On the contrary, in biofilm challenge mode, control samples and those treated with undoped-NPs decreased their *E** over time while Dox-NPs and Zn-NPs-treated specimens did not alter their resistance to dynamic deformation (Fig. 2).

3.3. Raman spectroscopy

Raman analysis results are shown in Table 2 and Fig. 3. Regarding the mineral content, Zn-NPs-treated dentin surfaces attained the highest mineralization degree related to the phosphate peak (960 cm^{-1}) at 72 h and 7 d time point, regardless the presence of biofilm challenge (Table 2). At 7 d of storage with biofilm challenge, demineralized dentin at the resin-dentin interface was present in all groups, as peaks at 431 cm^{-1} were higher than at 446 cm^{-1}. The lowest peak values at 579 and 590 cm^{-1} were attained in Zn-NPs-treated samples, after 7 d time point with biofilm challenge, indicating that dentin is mineralized. The lowest intensity ratio attained at 579/959, 590/959 corresponded to samples treated with Zn-NPs, demonstrating dentin remineralization at the interface (Table 2). Concerning the organic components, the highest Raman bands of the proline (937 cm^{-1}) and croslinking shifts corresponded to Zn-NPs-treated samples at 7 d of storage, with biofilm challenge. Regarding the collagen nature and secondary structure, Zn-NPs treated specimens attained the lowest amide-I/amide-III ratio (Table 2), at 7 d time point in biofilm challenge, linked to a raised mineralization effect. Dentin treated with Dox-NPs achieved and intermediate peak value (1.65 cm^{-1}), assessed at 7 d with biofilm challenge.

3.4. Field Emission Electron Microscopy (FESEM) analysis

Dentin surfaces FESEM examination revealed differences among groups (Fig. 3aSI-3hSI, Fig. 4a-4h). At 72 h of storage, the control group showed high density of bacteria beneath

the adhesive layer and at the intratubular dentin, where demineralized and non-resin infiltrated dentin was present (Fig. 3aSI). Demineralized collagen fibers and a bacterial consortium filling the tubule were shown at intratubular dentin, adhered to the demineralized collagen, in Fig. 3SIb. Bacterial consortium anchorage on unprotected and affected collagen was determined after 7 d time point in the control group (Figs. 4a, 4b). Undoped-NPs treated dentin interfaces showed empty areas, which were totally filled of bacteria, at 72 h time point (Figs. 3cSI, 3dSI). A dense cell community of the biofilm colonized the uncovered collagen, which appeared disrupted in some locations at 7 d storage (Figs. 4c, 4d). When Dox-NPs were used to infiltrate the dentin, the analysis revealed a profuse association between bacteria and NPs at the bottom of the hybrid layer at 72 h storage (Figs. 3eSI, 3fSI). After 7 d, a characteristic minimal amount of bacteria at the resin-dentin inter-diffusion area and the non-remineralized staggered collagen was observed (Figs. 4e, 4f). Zn-NPs promoted total remineralization of the non-resin covered collagen and bacteria were scarcely observed at 72 h and 7 d time points (Figs. 3gSI, 3hSI, 4g, 4h).

4. Discussion

An *in vitro* biological challenge involving a saliva-derived stock from plaque microcosm biofilm was selected in the present study, due to its clinical relevance [3,17,41]. Multispecies oral biofilms are preferred to simulate the complex actions produced on dental restorative materials [3,18,32].

Creation of a marginal gap, in which the bacteria could penetrate and grow, is crucial in the present experimental research. Then, selection of specimens designing (dentin cylinders of 5 mm) with a high C factor was preferred. Using root dentin instead of coronal dentin is recognized as a limitation of the present study, firstly because these two bonding substrates are different in both anatomical structure and bonding mechanisms, and secondly due to differences in pathogenic microorganism between coronal and intrarradicular dentin. Due to the high number of specimens needed in the present study bovine dentin was used instead of human dentin. However this procedure has been previously validated [17,18,42].

Tested NPs are non-degradable, so burst release is not produced. Zinc releasing values are 0.02 μg mL^{-1} (per mg of NPs) at 72 h and same values after 7d. Cumulative release is 0.8% for zinc after 28 d [29]. The tested Dox-NPs discs exhibited a controlled release of doxycycline at least over 28 days. For each mg of NPs 106 and 46 μg ml^{-1} of doxycycline was released at 24 and 48 h respectively, with the antibiotic release maintained above 20 μg ml^{-1} after 7 days [23]. Released concentrations of doxycycline from NPs will be high above to the antibacterial effective doses [24]. These values are calculated using a NPs immersion method. At the resin bonded interface, where the fluid-flow is reduced, even a slower release is expected to be produced. Moreover, it should be taken into account that zinc and doxycycline may also exert effect without been released, as NPs do not resorb.

Zinc release from NPs has been shown to be antimicrobial against cariogenic bacteria in planktonic cultures [29,23]. Cationic elements may displace other metal ions damaging the outer membrane, leading to cell death. Zinc has also a known inhibitory effect on glycolysis and proteinase activity in many oral bacteria [43]. Even when the exact antibacterial mechanism of zinc has not been clearly identified yet, oxidatively or covalently induced damage may occur. Zinc has long been known as a plaque-inhibiting compound and also can influence acid production by different microbes [24,44]. Application of Zn-NPs on acid etched dentin reduced biofilm formation and viability at the resin-dentin interface due to a combined effect, namely remineralization and antibacterial properties (after 7 d red stained cells -damaged bacteria- percentage was 87% and total detected bacteria was half if compared to undoped-NPs or control groups). Dox-NPs also diminished oral biofilm viability, 80% injured or dead cells after 72 h. LIVE/DEAD® images of samples treated indicated bacterial penetration into the resin-dentin interface (Fig. 1SI) (Table 1). On the contrary, at 7 d time point, control samples and those treated with undoped-NPs showed no anti-biofilm activity, with 46% and 51% of damaged or dead cells (Table 1; Fig. 1SI). These images confirmed the presence of poor dentin-adhesive interface integrity, that may be caused by the *in vitro* biofilm promoting acidic damage at the etched but non-resin infiltrated dentin [26]. This outcome denoted an anti-biofilm activity, mainly produced by Dox-NPs and Zn-NPs. In the case of Dox-NPs, antibacterial activity was

reduced from 24 h to 7 d to one third, however it should also be noted that the total bacterial counts at the bonded interface was reduced about five times. It is hypothesized that surviving bacteria after 7 d, were fewer in number, but most resistant to doxycycline effect. At the contrary in the case of Zn-NPs the total bacterial counts was similar after 24 h and 7 d, but the antibacterial activity (dead or injured cells) was almost two-fold after 7 d than at 24 h time-point, showing a slower antibacterial activity of Zn-NPs. It has been previously reported [41] that LIVE/DEAD® dyes may not be used as an exact quantitative measurement of cell death. Propidium iodide stained cells (red cells) may be falsely identified as dead cells, and represent cells that are injured, dead or starving viable cells. Therefore red cells percentages should be taken with caution. When analyzing FESEM images of those groups (Zn-NPs and Dox-NPs after 7 d), it is clear that bacteria were not easily observed at any of the bonded interfaces (Figs. 4b, 4d, 4g, 4h), corroborating LIVE/DEAD® results. In the rest of the groups, biofilm structures anchored and developed adherence and penetration through the BHL in dentin specimens incubated not only at 72 h, but also after 7 d (Figs. 3bSI, 3dSI). Dentin remineralization at the hybrid layer was encountered when Z-NPs were applied (Figs. 4g,4h). However, an advanced dentin demineralization was also observed at FESEM images of interfaces treated with Dox-NPs (Figs. 4b, 4d). Trough Raman analysis it was demonstrated that all groups reflected demineralization at the resin-dentin interface (Table 2), as the symmetric bending mode (v_2) of phosphate (PO_4^{3-}) at 431 cm^{-1} was greater than at 446 cm^{-1} peaks [37] in all cases.

It should be considered that NPs are not retained by physical absorption, but forming primary bonds with demineralized collagen. Dislodging during the dentin bonding will not occur as particle binding to demineralized collagen is produced. It may be explained by (1) the result of the high affinity between the negatively charged polymeric NPs (−43.3 mV) and the positively charged demineralized dentin collagen and (2) due to the binding of COO− groups from NPs to NH+ sites at dentin collagen. Then, particle retention at the demineralized dentin surface is produced, and it is important as NPs collagen binding is necessary to exert a remineralization effect [25,45]. It is also important to stress that tested NPs located at the resin-dentin bonded interface do not produce specific spectral features or fluorescence that may

overlap or obscure Raman signals, as previously demonstrated trough a detailed Raman analysis of the different substrates (polymers and dentin) at these bonded interfaces demonstrated [45]. Even when the complete Raman spectra were provided, just the relevant spectral features were assigned and commented in the present manuscript, some more information about Raman analysis of dentin bonded interface treated with the present experimental NPs is presented somewhere else [45].

Both the storage modulus (*E'*) and the loss modulus (*E''*) are involved in the viscoelastic expression of the complex modulus (*E**), only *E** will be discussed. The complex modulus is a measure of the material resistance to dynamic deformation [46]. The demineralized BHL is the Achilles's heel of adhesion to dentin, probably, which most likely determine the low restoration longevity [1]. At 7 d of storage, the BHL of specimens treated with Zn-NPs and exposed to biofilm challenge showed the highest *E** (Fig. 2), denoting advanced intrafibrillar remineralization [47]. Complex modulus outcomes show that the green and/or yellow regions observed at the bottom of the hybrid layer, when Zn-NPs were applied and analyzed after 7 d (Fig. 2aSI), had higher values than the rest of the specimens, suggesting the occurrence of minimal if any demineralization, and thus dentin remineralization [21] (Fig. 2). In general, complex modulus values of dentin treated with Zn-NPs were between two and four times fold those of control group, and it is consistent with other studies [31,45]. Zinc has been previously shown to produce calcium/phosphate precipitation and dentin remineralization with a high increase in mechanical properties [48]. It has also been shown when this new mineral is formed in the presence of zinc, an exchange between Zn^{2+} and Ca^{2+} occurs *in vitro*, forming a substituted apatite compound through an isomorphous substitution [49]. A higher nanohardness and lower solubility was found in this zinc-substituted mineralized layer [49,50].

Dentin treated with Zn-NPs after 7 d presents Raman bands at 579, 590, cm^{-1} (v_4 asymmetric bending mode PO_4^{3-}) reflected the lowest peak values among groups (Table 2), evoking the *in situ* presence of sound dentin [37]. The lowest intensity ratio plot showed at 579/ 959, 590/ 959 (Table 2), also demonstrated dentin remineralization at the interface [37,51]. This mineral precipitation promoted active dentin remodeling with increased maturity which was

sustained on a high collagen quality parameter (1.37) (ratio 1674 cm^{-1}/1690 cm^{-1}) [40] (Table 2) and higher mechanical properties [31,45]. These new mineral formations, absent in the rest of the groups, were observed as multiple rod-like figures that filled the intratubular dentin lumen at both peritubular and intertubular dentin [45] (Fig. 4h).

To prevent stress concentration zones and to avoid crack propagation across the surface, the remineralized dentin should absorb mechanical shock waves. *E** results revealed that there is homogeneity in the mechanical properties distribution between HL and BHL, when samples were treated with both Dox-NPs and Zn-NPs (Fig. 2). HL in both groups showed higher *E** than the BHL (1.28 and 1.03 fold, respectively) enabling, thereby, the energy dissipation across their structures. Thus, at 7 d of storage, nano-DMA revealed that there is heterogeneity in the mechanical properties distribution at both HL and BHL in the group of samples treated with Dox-NPs, exposed to biofilm challenge, making the tissue prone to cracking [52,53]. This breakdown of dentin, preferentially occurred at the HL [54], precisely where bands at 579, 590, cm^{-1} showed the highest peak values (41.68 and 38.75, respectively), which suggests the greatest demineralization zone [37] among all groups (Table 2). The failure coincided with the formed gap in the resin-dentin interface which clearly caused the HL to be detached from the BHL (Fig. 4e). The presence of these cracks supports the assumption that the cracks can facilitate acids penetration. However, secondary caries formation may be impaired [55], due to both the inhibitory effect of MMPs by doxycycline [56] and the antibacterial properties of Dox-NPs [23,24].

Dox-NPs application did not induce minerals precipitation or dentin remineralization (Fig. 3) [31]. However, the reinforced dentin microstructure and the relatively improved mechanical properties (Fig. 2) are probably due to the high collagen-crosslinking that was obtained after Dox-NPs application [45,57,58] (Table 2). The main component of AGE (advance glycation end products) is the pentosidine [40]. Pentosidine Raman signal attained the highest values in Zn-NPs-treated samples (14.38) (Table 2) when compared with the rest of groups, indicating advanced scaffolding of collagen and greater potential for further remineralization [40]. Even at 72 h of storage, Dox-NPs-treated dentin attained the lowest

storage modulus (Fig. 2fSI) (Table 1SI) with minimal remineralization (Figs. 3SIe, 3SIf). Raman peaks detected at 1400cm^{-1} correspond to bonds of Ca-COO and can be associated with Ca-Dox complexes that affect the primary nucleation, interfering with mineral precipitation and inhibiting mineralization [59]. Ca-COO peaks became higher over time (Fig. 3f), and this ability to chelate calcium ions, may be responsible for some deterioration of the mechanical properties [59] (Fig. 2). The initial burst of Doxycycline release from NPs, which has been previously described [23] was confirmed by the hierarchical cluster analysis (HCA) of the Raman spectra after 72 h (Fig. 3c). The three plots corresponded to the different HCA variances that appeared below 750 cm^{-1} Raman shifts. They still appeared but became lower after 7 d (Fig. 3d), probably indicating minor drug release from the delivery system after this time (NPs) [23,59]. At 7 d of storage, Dox presence increased at the resin-dentin interface and so the Dox-Ca complexes (Fig. 3f). This outcome warranted the antibacterial properties [24] of Dox-NPs over time.

The lower nano-DMA outcomes when both control or undoped-NPs groups were exposed to biofilm challenge 7 d correlated with revealed areas of demineralization (Figs. 4b, 4d, respectively) as a product of incomplete resin impregnation of demineralized dentin. Even at 72 h of storage, undoped-NPs treated dentin showed the lowest loss modulus, among groups at both the HL (2.61 GPa) and the BHL (2.51 GPa) (Table 1SI) (Fig. 2gSI). This also correlated with the high RMC values (Table 2) that were obtained after applying unloaded-NPs. RMC expresses the relative presence of minerals [phosphate, (PO_4^{3-})] referred to proteins (phenyl group), [60]. The Raman peak of phenyl in dentin treated with undoped-NPs showed the low intensity that was obtained in the present study (43.06) among the groups in which NPs were applied (Table 2). This fact reflected the presence of scarce matrix content and damaged collagen (Figs. 4c, 4d), which indirectly raised the quotient RMC (Table 2) [57]. The lack of resin infiltration and proper dentin remineralization in specimens treated with undoped-NPs allow the bacteria to have access to colonize the demineralized dentin collagen, along the interface [61] (Figs. 4b, 4d). As a result, bacteria could penetrate through the demineralized pores, voids, cracks and open tubules [31] allowing the presence of mature biofilm within the structures of the resin-dentin interface, even at 72 h of storage (Figs 4b, 4d, 3bSI, 3dSI).

Accordingly, it is speculated that bacteria and the existence of demineralized dentin at the BHL, may synergistically promote secondary tooth caries formation. The bonded interface is then degraded by oral bacteria leakage at the gaps of the BHL. Bacteria can directly colonize and bind to demineralized collagen present in dentin [2], forming a biofilm and infecting the dentinal tissues [17]. Bacteria, through adhesins present at the cell membrane and in junction with other collagen-binding protein and serine proteases, anchorage and colonize the non-resin covered or unprotected collagen, where they exert their proteolytic and demineralizing action [32,62], promoting interfacial degradation.

Zinc and doxycycline are antibacterial [63] and also potent matrix metalloproteinases (MMPs) inhibitors; thereby, they are collagen protectors [56]. This point has gained clinical relevance after studies performed by Finer, as it was demonstrated that dentinal pathogenic bacteria produce MMPs that may degrade collagen facilitating dentin invasion [64]. Consistent with these results it was also shown that a MMPs inhibitor with no antibacterial activity was able to enhance marginal integrity and to reduce interfacial bacterial ingress and bacterial biomass in dentin-resin bonded interfaces [65].

The mineral precipitation in specimens treated with Zn-NPs (Fig. 4h) lead to a reduced bacterial penetration, when compared with those treated with Dox-NPs (Fig. 4f), after 7 d of biofilm challenge. Therefore, the remineralizing and antibacterial effects were combined when Zn-NPs were applied. In this manuscript, we have attained a positive outcome in one of the highest noteworthy areas of concern in adhesive dentistry, the stability of the dentin bonding interface. This work provides a framework for further research trying to develop future materials with intrinsic antimicrobial effects, and materials which will not only functionally restore dentin but also stimulate biological responses that increase remineralization and natural dentin repair [66].

The present study used a multispecies biofilm from a stock of plaque microcosm biofilm. This complex and clinically relevant biofilm provides experimental conditions that can be used to assess the potential clinical efficacy of the experimental NPs [41]. However, it is important to note that the antimicrobial NPs do not selectively kill certain pathogens. They act

as broad spectrum antimicrobials. As such, they indiscriminately will affect commensal bacteria, which can compromise the balance of species in the healthy oral biofilm. Further research about potential effects on biofilm dysbiosis should be performed.

The present research is new not only regarding the use of these unique loaded NPs but also, because of the multiple complementary research testing and characterization techniques and tools performed to evaluate the effect of the bacterial challenge, at the bonded resin-dentin interface. Nanomechanical, morphological and chemical considerations were innovatively taken together to analyze the data and draw conclusions.

The results of this research are clinically relevant. But this study also has some limitations: 1) antibiotics may produce bacterial resistance and dysbiosis which are current global concerns; therefore, further research is needed to ascertain the long-term effect of tested NPS at the bonded interface, 2) the employed drip flow reactor does not take into consideration the effect of mechanical loading in gap formation, bacterial penetration and the consequent demineralization, it deserves future research, 3) the use of bovine radicular dentin, 3) the perpendicular direction of the dentinal tubules respect to the bonded interface which varies from the orientation found in real clinical conditions and 4) creating cavities with a high C factor, favoring gaps formation and bacterial colonization. This implies that caution must be implemented when trying to extrapolate the current outcomes to clinical conditions. Future clinical studies focusing on the resin-dentin interface degradation are encouraged.

5. Conclusions

The combined antibacterial and remineralizing effects of Zn-NPs at the dentin interface decreased the hybrid layer degradation mediated by the tested *in vitro* cariogenic biofilm. There was a significant bacterial viability reduction, over time, when Dox-NPs were applied. Application of Dox-NPs on dentin also produced advanced scaffolding of collagen but did not facilitate resin-dentin interface remineralization.

Disclosure

The authors report no conflicts of interest in this work.

Acknowledgements

This work was supported by the Ministry of Economy and Competitiveness and European Regional Development Fund [MAT2017-85999P MINECO/AEI/FEDER/UE] and University of Granada Research & Transfer Program. The authors acknowledge Professor Joel D. Rudney, University of Minnesota for facilitating the use of microbiology facilities and access to the plaque samples. Multiphoton confocal laser microscope was performed at the University of Minnesota Imaging Centers (http://uic.umn.edu).

References

[1] P. Spencer, Q. Ye, J. Park, E.M. Topp, A. Misra, O. Marangos, Y. Wang, B.S. Bohaty, V. Singh, F. Sene, J. Eslick, K. Camarda, J.L. Katz, Adhesive/Dentin interface: the weak link in the composite restoration, Ann. Biomed. Eng. 38 (2010) 1989–2003.

[2] S. Kermanshahi, J.P. Santerre, D.G. Cvitkovitch, Y. Finer, Biodegradation of Resin-Dentin Interfaces Increases Bacterial Microleakage, J. Dent. Res. 89 (2010) 996–1001.

[3] J.L. Ferracane, Models of Caries Formation around Dental Composite Restorations, J. Dent. Res. 96 (2017) 364–371.

[4] P. Spencer, Q. Ye, L. Song, R. Parthasarathy, K. Boone, A. Misra, C. Tamerler, Threats to adhesive/dentin interfacial integrity and next generation bio-enabled multifunctional adhesives, J. Biomed. Mater. Res. B Appl. Biomater. 107 (2019) 2673–2683.

[5] Y. Wang, P. Spencer, M.P. Walker, Chemical profile of adhesive/caries-affected dentin interfaces using Raman microspectroscopy, J. Biomed. Mater. Res. A. 81 (2007) 279–286.

[6] J.H. Kinney, S.J. Marshall, G.W. Marshall, The mechanical properties of human dentin: a critical review and re-evaluation of the dental literature, Crit. Rev. Oral Biol. Med. Off. Publ. Am. Assoc. Oral Biol. 14 (2003) 13–29.

[7] N. Nakabayashi, D.H. Pashley, Hybridization of dental hard tissues, Quintessence Pub. Co., Tokyo; Chicago, 1998.

[8] D.H. Pashley, F.R. Tay, C. Yiu, M. Hashimoto, L. Breschi, R.M. Carvalho, S. Ito, Collagen degradation by host-derived enzymes during aging, J. Dent. Res. 83 (2004) 216–221.

[9] A.P. Fugolin, A. Dobson, V. Huynh, W. Mbiya, O. Navarro, C.M. Franca, M. Logan, J.L. Merritt, J.L. Ferracane, C.S. Pfeifer, Antibacterial, Ester-Free Monomers: Polymerization Kinetics, Mechanical Properties, Biocompatibility and Anti-Biofilm Activity, Acta Biomater. 100 (2019) 132–141.

[10] E.A. Kidd, D. Beighton, Prediction of secondary caries around tooth-colored restorations: a clinical and microbiological study, J. Dent. Res. 75 (1996) 1942–1946.

[11] K.K. Choi, J.R. Condon, J.L. Ferracane, The effects of adhesive thickness on polymerization contraction stress of composite, J. Dent. Res. 79 (2000) 812–817.

[12] J.A. Aas, A.L. Griffen, S.R. Dardis, A.M. Lee, I. Olsen, F.E. Dewhirst, E.J. Leys, B.J. Paster, Bacteria of Dental Caries in Primary and Permanent Teeth in Children and Young Adults, J. Clin. Microbiol. 46 (2008) 1407–1417.

[13] R.H. Selwitz, A.I. Ismail, N.B. Pitts, Dental caries, Lancet Lond. Engl. 369 (2007) 51–59.

[14] P.H. Keyes, Research in dental caries, J. Am. Dent. Assoc. 76 (1968) 1357–1373.

[15] P.H. Keyes, The infectious and transmissible nature of experimental dental caries: Findings and implications, Arch. Oral Biol. 1 (1960) 304-IN4.

[16] R.M. Stephan, Intra-oral hydrogen-ion concentrations associated with dental caries activity., J. Dent. Res. 23 (1944) 257–266.

[17] D.G. Moussa, A. Fok, C. Aparicio, Hydrophobic and antimicrobial dentin: A peptide-based 2-tier protective system for dental resin composite restorations, Acta Biomater. 88 (2019) 251–265.

[18] Y. Li, C. Carrera, R. Chen, J. Li, P. Lenton, J.D. Rudney, R.S. Jones, C. Aparicio, A. Fok, Degradation in the dentin–composite interface subjected to multi-species biofilm challenges, Acta Biomater. 10 (2014) 375–383.

[19] Q. Ye, P. Spencer, E. Yuca, C. Tamerler, Engineered Peptide Repairs Defective Adhesive–Dentin Interface, Macromol. Mater. Eng. 302 (2017) 1600487.

[20] A.L. Medina-Castillo, J.F. Fernandez-Sanchez, A. Segura-Carretero, A. Fernandez-Gutierrez, Micrometer and Submicrometer Particles Prepared by Precipitation Polymerization: Thermodynamic Model and Experimental Evidence of the Relation between Flory's Parameter and Particle Size, Macromolecules. 43 (2010) 5804–5813.

[21] D. Khvostenko, T.J. Hilton, J.L. Ferracane, J.C. Mitchell, J.J. Kruzic, Bioactive glass fillers reduce bacterial penetration into marginal gaps for composite restorations, Dent. Mater. Off. Publ. Acad. Dent. Mater. 32 (2016) 73–81.

[22] R. Osorio, I. Cabello, A.L. Medina-Castillo, E. Osorio, M. Toledano, Zinc-modified nanopolymers improve the quality of resin-dentin bonded interfaces, Clin. Oral Investig. 20 (2016) 2411–2420.

[23] M. Toledano-Osorio, J.P. Babu, R. Osorio, A.L. Medina-Castillo, F. García-Godoy, M. Toledano, Modified Polymeric Nanoparticles Exert In Vitro Antimicrobial Activity Against Oral Bacteria, Materials. 11 (2018) 1013.

[24] M.C. Sánchez, M. Toledano-Osorio, J. Bueno, E. Figuero, M. Toledano, A.L. Medina-Castillo, R. Osorio, D. Herrera, M. Sanz, Antibacterial effects of polymeric PolymP-n Active nanoparticles. An in vitro biofilm study, Dent. Mater. 35 (2019) 156–168.

[25] R. Osorio, E. Osorio, A.L. Medina-Castillo, M. Toledano, Polymer Nanocarriers for Dentin Adhesion, J. Dent. Res. 93 (2014) 1258–1263.

[26] M.A. Melo, S. Orrego, M.D. Weir, H.H.K. Xu, D.D. Arola, Designing Multiagent Dental Materials for Enhanced Resistance to Biofilm Damage at the Bonded Interface, ACS Appl. Mater. Interfaces. 8 (2016) 11779–11787.

[27] M.M. Mutluay, K. Zhang, H. Ryou, M. Yahyazadefar, H. Majd, H.H.K. Xu, D. Arola, On the Fatigue Behavior of Resin-Dentin Bonds after Degradation by Biofilm, J. Mech. Behav. Biomed. Mater. 18 (2013) 219–231.

[28] A.C.-T. Ko, M. Hewko, M.G. Sowa, C.C.S. Dong, B. Cleghorn, L.-P. Choo-Smith, Early dental caries detection using a fibre-optic coupled polarization-resolved Raman spectroscopic system, Opt. Express. 16 (2008) 6274–6284.

[29] R. Osorio, C.A. Alfonso-Rodríguez, A.L. Medina-Castillo, M. Alaminos, M. Toledano, Bioactive Polymeric Nanoparticles for Periodontal Therapy, PloS One. 11 (2016) e0166217.

[30] M. Toledano, M. Toledano-Osorio, M.D. Navarro-Hortal, A. Varela-López, R. Osorio, J.L. Quiles, Novel Polymeric Nanocarriers Reduced Zinc and Doxycycline Toxicity in the Nematode Caenorhabditis elegans, Antioxid. Basel Switz. 8 (2019) E550.

[31] M. Toledano-Osorio, E. Osorio, F.S. Aguilera, A.L. Medina-Castillo, M. Toledano, R. Osorio, Improved reactive nanoparticles to treat dentin hypersensitivity, Acta Biomater. 72 (2018) 371–380.

[32] C.A. Carrera, Y. Li, R. Chen, C. Aparicio, A. Fok, J. Rudney, Interfacial degradation of adhesive composite restorations mediated by oral biofilms and mechanical challenge in an extracted tooth model of secondary caries, J. Dent. 66 (2017) 62–70.

[33] J.D. Rudney, R. Chen, P. Lenton, J. Li, Y. Li, R.S. Jones, C. Reilly, A.S. Fok, C. Aparicio, A reproducible oral microcosm biofilm model for testing dental materials, J. Appl. Microbiol. 113 (2012) 1540–1553.

[34] L. Han, A.J. Grodzinsky, C. Ortiz, Nanomechanics of the Cartilage Extracellular Matrix, Annu. Rev. Mater. Res. 41 (2011) 133–168.

[35] J.W. Ager, R.K. Nalla, K.L. Breeden, R.O. Ritchie, Deep-ultraviolet Raman spectroscopy study of the effect of aging on human cortical bone, J. Biomed. Opt. 10 (2005) 034012.

[36] J.F. McCabe, A.W.G. Walls, eds., Applied Dental Materials, 9 edition, Wiley-Blackwell, Oxford, UK ; Ames, Iowa, 2008.

[37] A.C.-T. Ko, L.-P. Choo-Smith, M. Hewko, L. Leonardi, M.G. Sowa, C.C.S. Dong, P. Williams, B. Cleghorn, Ex vivo detection and characterization of early dental caries by optical coherence tomography and Raman spectroscopy, J. Biomed. Opt. 10 (2005) 031118.

[38] A.R. Hunter, E.T. Treasure, A.J. Hunter, Increases in cavity volume associated with the removal of class 2 amalgam and composite restorations., Oper. Dent. 20 (1995) 2–6.

[39] D.R. Sell, V.M. Monnier, Structure elucidation of a senescence cross-link from human extracellular matrix. Implication of pentoses in the aging process, J. Biol. Chem. 264 (1989) 21597–21602.

[40] H. Salehi, E. Terrer, I. Panayotov, B. Levallois, B. Jacquot, H. Tassery, F. Cuisinier, Functional mapping of human sound and carious enamel and dentin with Raman spectroscopy, J. Biophotonics. 6 (2013) 765–774.

[41] J. Kreth, J.L. Ferracane, C.S. Pfeifer, S. Khajotia, J. Merritt, At the Interface of Materials and Microbiology: A Call for the Development of Standardized Approaches to Assay Biomaterial-Biofilm Interactions, J. Dent. Res. 98 (2019) 850–852.

[42] Y. Li, C. Carrera, R. Chen, J. Li, Y. Chen, P. Lenton, J.D. Rudney, R.S. Jones, C. Aparicio, A. Fok, Fatigue failure of dentin-composite disks subjected to cyclic diametral compression, Dent. Mater. Off. Publ. Acad. Dent. Mater. 31 (2015) 778–788.

[43] M. Tamura, K. Ochiai, Zinc and copper play a role in coaggregation inhibiting action of Porphyromonas gingivalis, Oral Microbiol. Immunol. 24 (2009) 56–63.

[44] D. Wunder, W.H. Bowen, Action of agents on glucosyltransferases from Streptococcus mutans in solution and adsorbed to experimental pellicle, Arch. Oral Biol. 44 (1999) 203–214.

[45] M. Toledano, R. Osorio, E. Osorio, A.L. Medina-Castillo, M. Toledano-Osorio, F.S. Aguilera, Ions-modified nanoparticles affect functional remineralization and energy dissipation through the resin-dentin interface, J. Mech. Behav. Biomed. Mater. 68 (2017) 62–79.

[46] H. Ryou, D.H. Pashley, F.R. Tay, D. Arola, A characterization of the mechanical behavior of resin-infiltrated dentin using nanoscopic Dynamic Mechanical Analysis, Dent. Mater. Off. Publ. Acad. Dent. Mater. 29 (2013) 719–728.

[47] J.H. Kinney, S.J. Marshall, G.W. Marshall, The mechanical properties of human dentin: a critical review and re-evaluation of the dental literature, Crit. Rev. Oral Biol. Med. Off. Publ. Am. Assoc. Oral Biol. 14 (2003) 13–29.

[48] R. Osorio, M. Toledano-Osorio, E. Osorio, F.S. Aguilera, S. Padilla-Mondéjar, M. Toledano, Zinc and silica are active components to efficiently treat in vitro simulated eroded dentin, Clin. Oral Investig. 22 (2018) 2859–2870.

[49] R. Osorio, E. Osorio, I. Cabello, M. Toledano, Zinc induces apatite and scholzite formation during dentin remineralization, Caries Res. 48 (2014) 276–290.

[50] S.R. Vasant, M.J. Joshi, Synthesis and characterization of pure and zinc doped calcium pyrophosphate dihydrate nanoparticles, Eur. Phys. J. - Appl. Phys. 53 (2011).

[51] M. Toledano, E. Osorio, F.S. Aguilera, I. Cabello, M. Toledano-Osorio, R. Osorio, Ex vivo detection and characterization of remineralized carious dentin, by nanoindentation and single point Raman spectroscopy, after amalgam restoration, J. Raman Spectrosc. 48 (2017) 384–392.

[52] R. Agrawal, A. Nieto, H. Chen, M. Mora, A. Agarwal, Nanoscale damping characteristics of boron nitride nanotubes and carbon nanotubes reinforced polymer composites, ACS Appl. Mater. Interfaces. 5 (2013) 12052–12057.

[53] V. Gopalakrishnan, C.F. Zukoski, Delayed flow in thermo-reversible colloidal gels, J. Rheol. 51 (2007) 623–644.

[54] D.M. Espino, D.E.T. Shepherd, D.W.L. Hukins, Viscoelastic properties of bovine knee joint articular cartilage: dependency on thickness and loading frequency, BMC Musculoskelet. Disord. 15 (2014) 205.

[55] N.M.S. Leal, J.L. Silva, M.I.M. Benigno, E.A. Bemerguy, J.B.C. Meira, R.Y. Ballester, How mechanical stresses modulate enamel demineralization in non-carious cervical lesions?, J. Mech. Behav. Biomed. Mater. 66 (2017) 50–57.

[56] R. Osorio, M. Yamauti, E. Osorio, M.E. Ruiz-Requena, D.H. Pashley, F.R. Tay, M. Toledano, Zinc reduces collagen degradation in demineralized human dentin explants, J. Dent. 39 (2011) 148–153.

[57] M. Toledano, I. Cabello, E. Osorio, F.S. Aguilera, A.L. Medina-Castillo, M. Toledano-Osorio, R. Osorio, Zn-containing polymer nanogels promote cervical dentin remineralization, Clin. Oral Investig. 23 (2019) 1197–1208.

[58] K.-D. Liss, A. Bartels, A. Schreyer, H. Clemens, High-energy X-rays: a tool for advanced bulk investigations in materials science and physics, Textures Microstruct. 35 (2003) 219–252.

[59] F. Tamimi, J. Torres, R. Bettini, F. Ruggera, C. Rueda, M. López- Ponce, E. Lopez-Cabarcos, Doxycycline sustained release from brushite cements for the treatment of periodontal diseases, J. Biomed. Mater. Res. A. 85A (2008) 707–714.

[60] A.G. Schwartz, J.D. Pasteris, G.M. Genin, T.L. Daulton, Stavros Thomopoulos, Mineral distributions at the developing tendon enthesis, PloS One. 7 (2012) e48630.

[61] D. Khvostenko, S. Salehi, S.E. Naleway, T.J. Hilton, J.L. Ferracane, J.C. Mitchell, J.J. Kruzic, Cyclic mechanical loading promotes bacterial penetration along composite restoration marginal gaps, Dent. Mater. Off. Publ. Acad. Dent. Mater. 31 (2015) 702–710.

[62] I. Nedeljkovic, W. Teughels, J. De Munck, B. Van Meerbeek, K.L. Van Landuyt, Is secondary caries with composites a material-based problem?, Dent. Mater. Off. Publ. Acad. Dent. Mater. 31 (2015) e247-277.

[63] T.-S. Kim, T. Bürklin, B. Schacher, P. Ratka-Krüger, M.T. Schaecken, H.H. Renggli, W. Fiehn, P. Eickholz, Pharmacokinetic Profile of a Locally Administered Doxycycline Gel in Crevicular Fluid, Blood, and Saliva, J. Periodontol. 73 (2002) 1285–1291.

[64] M.Q. Marashdeh, R. Gitalis, C. Lévesque, Y. Finer, Endodontic pathogens possess collagenolytic properties that degrade human dentine collagen matrix, Int. Endod. J. 52 (2019) 416–423.

[65] B. Huang, D.G. Cvitkovitch, J.P. Santerre, Y. Finer, Biodegradation of resin-dentin interfaces is dependent on the restorative material, mode of adhesion, esterase or MMP inhibition, Dent. Mater. Off. Publ. Acad. Dent. Mater. 34 (2018) 1253–1262.

[66] S.C. Bayne, J.L. Ferracane, G.W. Marshall, S.J. Marshall, R. van Noort, The Evolution of Dental Materials over the Past Century: Silver and Gold to Tooth Color and Beyond, J. Dent. Res. 98 (2019) 257–265.

Table 1. Mean and standard deviation of total areas occupied by bacteria (pixels) and percentages (%) of the LIVE/DEAD® assessed at the resin-dentin interfaces of the different experimental groups.

	Total (pixels) Mean (SD)	Live Cells Green (%) Mean (SD)	Dead/Injured Cells Red (%) Mean (SD)
No NPs / 72 h	3437.23 (862.46)	0.69 (0.11)	0.31 (0.11)
No NPs / 7 d	3930.29 (1534.24)	0.54 (0.01)	0.46 (0.01)
Undoped-NPs / 72 h	3790.95 (927.80)	0.55 (0.02)	0.45 (0.02)
Undoped-NPs / 7 d	3757.93 (1112.67)	0.49 (0.11)	0.51 (0.11)
Dox-NPs / 72 h	3705.83 (704.21)	0.20 (0.11)	0.80 (0.11)
Dox-NPs / 7 d	680.27 (786.74)	0.68 (0.23)	0.32 (0.23)
Zn-NPs / 72 h	4528.18 (2484.17)	0.47 (0.03)	0.53 (0.03)
Zn-NPs / 7 d	2405.69 (1368.88)	0.13 (0.04)	0.87 (0.04)

Table 2. Raman intensity (in arbitrary units) at the resin-dentin interfaces.

			No NPs				Undoped-NPs				Dox-NPs				Zn-NPs			
			72h		7d		72h		7d		72h		7d		72h		7d	
			No biofilm	Biofilm Challenge	No biofilm	Biofilm Challenge	No biofilm	Biofilm Challenge	No biofilm	Biofilm Challenge	No biofilm	Biofilm Challenge	No biofilm	Biofilm Challenge	No biofilm	Biofilm Challenge	No biofilm	Biofilm Challenge
MINERAL COMPONENTS																		
Relative Presence of Mineral	**Phosphate [959]**	**Peak**	120.50	137.78	191.22	369.04	130.63	333.78	109.71	250.34	254.48	313.46	256.88	321.98	329.69	364.02	279.62	417.01
		RMC	6.30	15.76	2.91	13.77	4.39	7.96	2.05	5.81	11.34	6.79	7.49	7.60	5.27	9.82	3.71	4.43
v_2 [430-431]			18.62	20.71	21.45	63.91	25.32	38.2387	19.96	43.02	291.35	302.85	150.14	112.90	44.43	70.01	56.90	93.54
v_2 [446]			12.45	14.85	11.04	53.04	16.90	28.4414	14.54	32.54	283.98	333.52	140.01	97.02	29.90	58.59	43.92	75.86
v_4 [579]			7.58	10.52	17.25	23.14	8.26	39.0565	8.98	19.28	150.02	157.55	66.08	41.68	25.52	55.04	16.17	13.85
v_4 [590]			22.31	22.61	69.36	36.00	19.66	55.4714	60.41	34.57	188.04	170.89	83.26	38.75	36.49	59.67	67.96	19.92
Ratio [579]/[959]			0.06	0.08	0.09	0.06	0.06	0.12	0.08	0.08	0.59	0.50	0.26	0.13	0.08	0.15	0.06	0.03
Ratio [590]/[959]			0.19	0.16	0.36	0.10	0.15	0.17	0.55	0.14	0.74	0.55	0.32	0.12	0.11	0.16	0.24	0.05
ORGANIC COMPONENTS																		
Collagen	**Proline [937]**		35.63	33.65	100.01	66.96	54.02	81.57	83.75	59.93	74.92	86.42	61.23	85.03	93.01	64.50	116.59	131.35
Normalization	**Phenyl [1003]**		19.14	8.74	65.81	26.80	29.79	41.94	53.43	43.06	22.43	46.18	34.31	42.35	62.54	37.07	75.30	94.15
Crosslinking	**AGEs-Pentosidine [1550]**		3.93	4.65	6.56	4.37	3.03	4.44	6.79	3.04	8.85	12.67	7.53	10.38	5.39	2.89	4.74	14.38
Nature and secondary structure of collagen	**Ratio A-I [1674]/ A-III [1690]**		1.30	2.31	2.23	1.69	1.81	3.22	1.97	2.17	1.97	2.61	1.62	1.65	2.16	1.65	1.73	1.37

RMC: Relative Mineral Concentration between mineral [959 cm^{-1}]/Phenyl [1003 cm^{-1}]; A: amide; AGEs: advanced glycation end products. Peaks positions are expressed in cm^{-1}. The peaks values have been normalized to the basis intensity of the CH_2 band [1452], near 1500 cm^{-1}.

Figure 1.

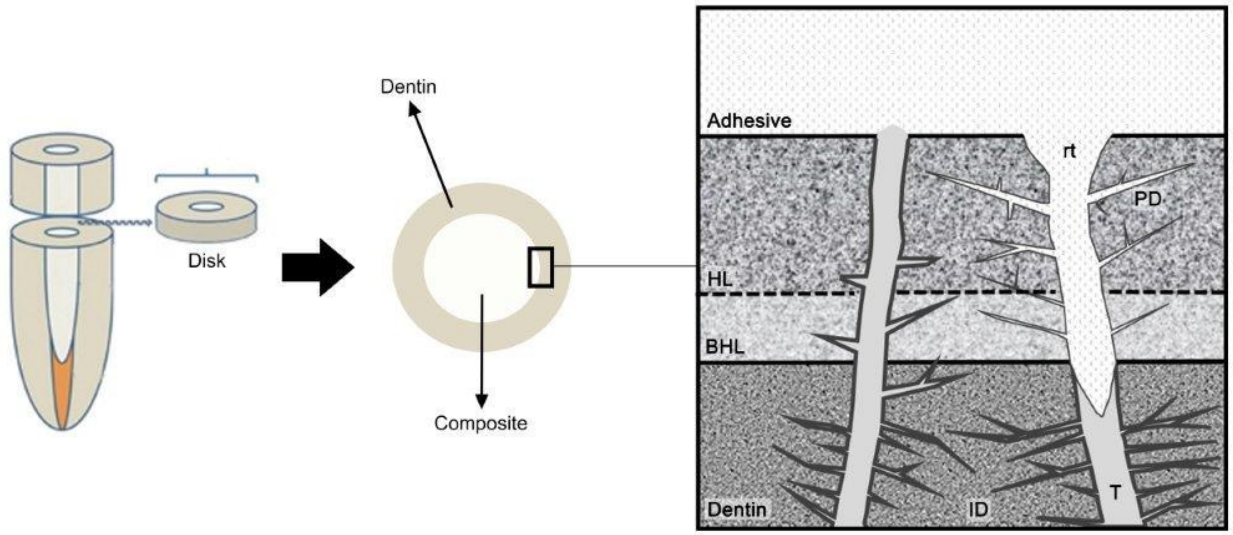

Figure 1. Schematic illustration presenting disks preparation mode and the observation zone for all experimental procedures (the resin-dentin bonded interface). Regions of interest for analysis were selected just below the adhesive layer. HL: Hybrid Layer; BHL: Bottom of Hybrid Layer; PD: Peritubular Dentin; ID: Intertubular Dentin; rt: resin tag; T: dentinal tubule.

Figure 2.

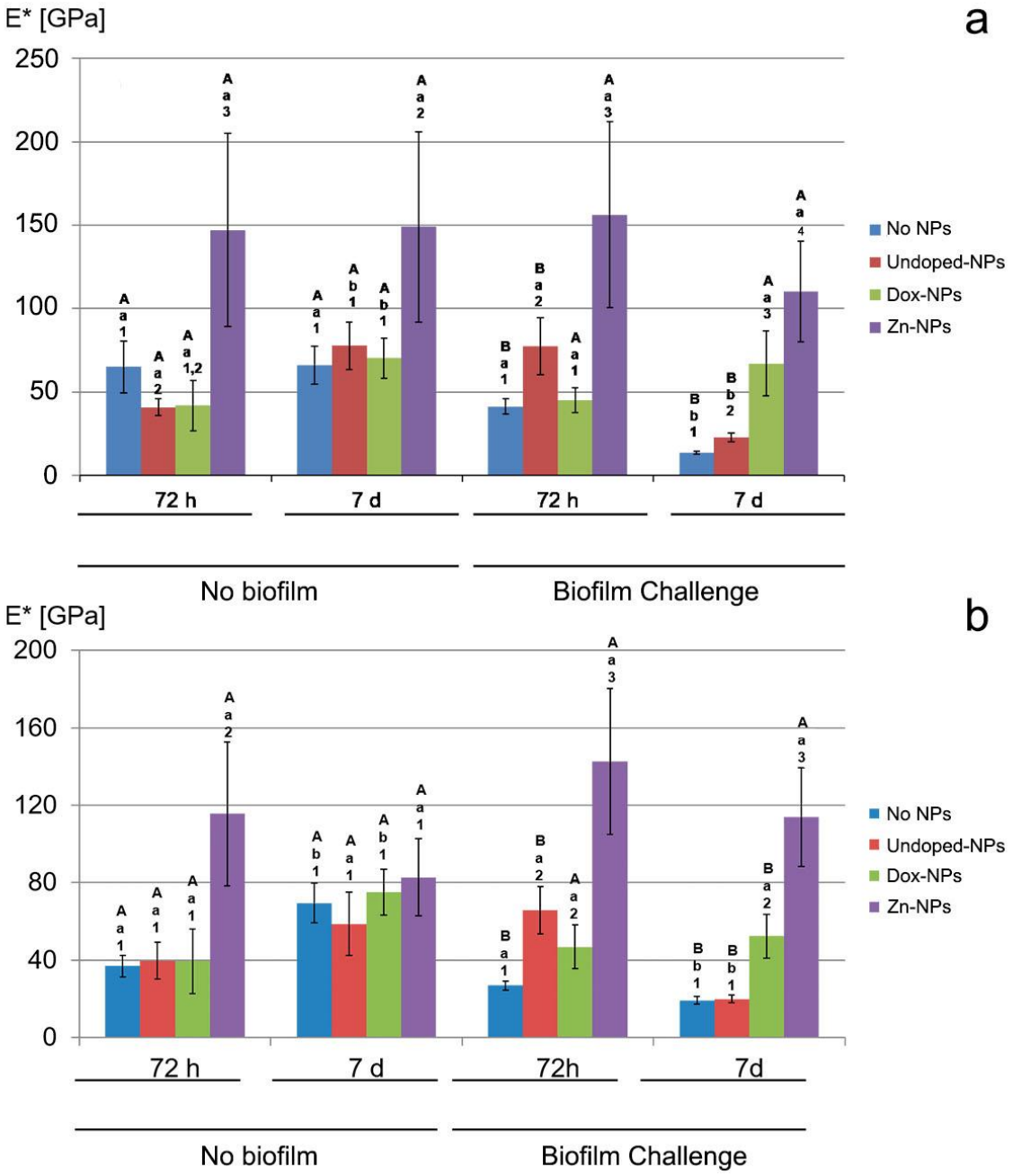

Figure 2. (**a,b**) Complex Modulus (GPa) at the different resin-dentin bonded interfaces, measured at both hybrid layer (HL) **(a)** and bottom of hybrid layer (BHL) **(b)** locations respectively. HL and BHL were analyzed independently. Similar capital letters indicate no significant differences between biofilm groups within the same NPs group and time-points ($p<0.01$). Comparisons within the same biofilm and NPs groups are indicated with similar lowercase letters, indicating no significant differences between time-points (72 h and 7 d of storage) ($p<0.01$). Numbers indicate significant differences among NPs groups, within the same biofilm and time-points groups ($p<0.05$).

Figure 3.

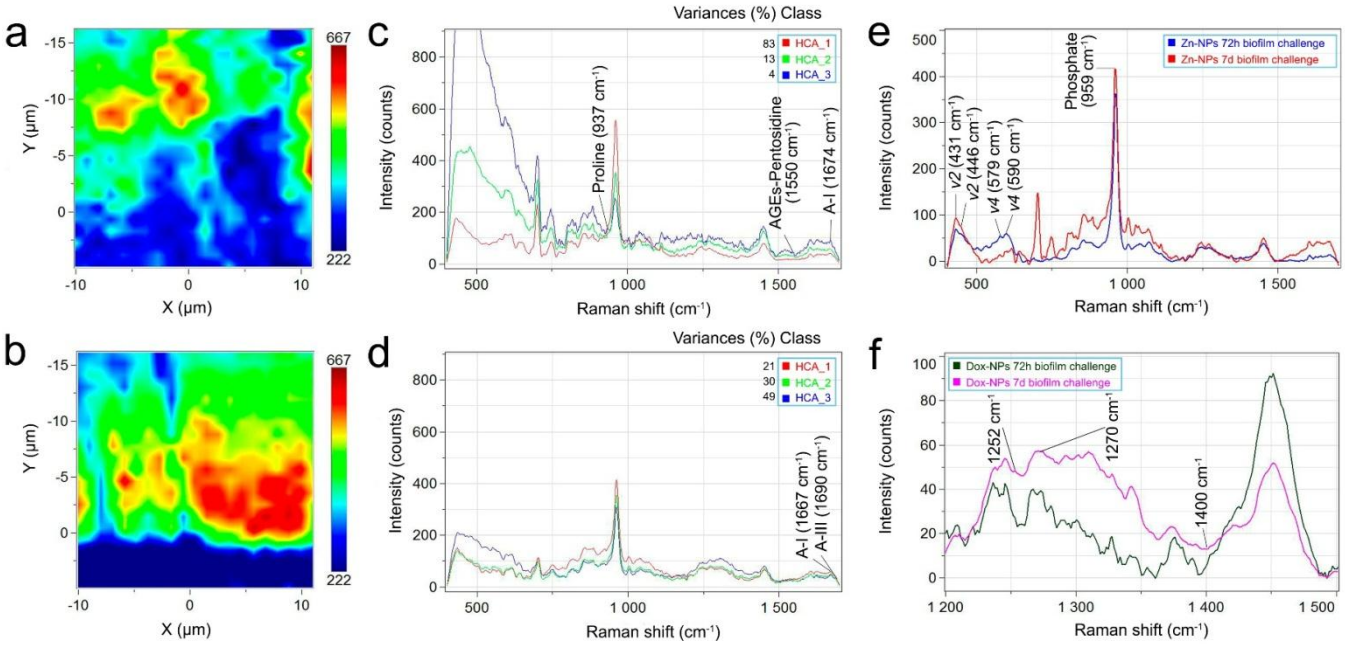

Figure 3. 2D micro-Raman map (20 x 20 µm) of the phosphate peak (961 cm^{-1}) intensities at the resin-dentin interface obtained after Dox-NPs (**a**) and Zn-NPs (**b**) application, at 7 d of storage with biofilm challenge. Raman spectra from hierarchical cluster analysis (HCA) results of samples treated with Dox-NPs, at 72 h (**c**), 7 d (**d**) of storage with biofilm challenge. Three levels of HCA clustering are shown. Variances of distinct colors have differences in Raman spectral distribution and chemical composition. Each percentage cluster is assigned to a different color (red, green and blue). Raman spectra from hierarchical cluster analysis (HCA) results at the hybrid layer of samples treated with Zn-NPs, at 72 h and 7 d of storage with biofilm challenge (**e**). A truncated segment (1200-1500 Raman shits, cm^{-1}) of micro-Raman analysis (**f**) corresponding to the double peak of doxycycline (1252 cm^{-1}, 1270 cm^{-1}) and calcium-doxycycline complexes (1400 cm^{-1}) at both 72 h and 7 d storage time in biofilm challenge, may be observed.

Figure 4.

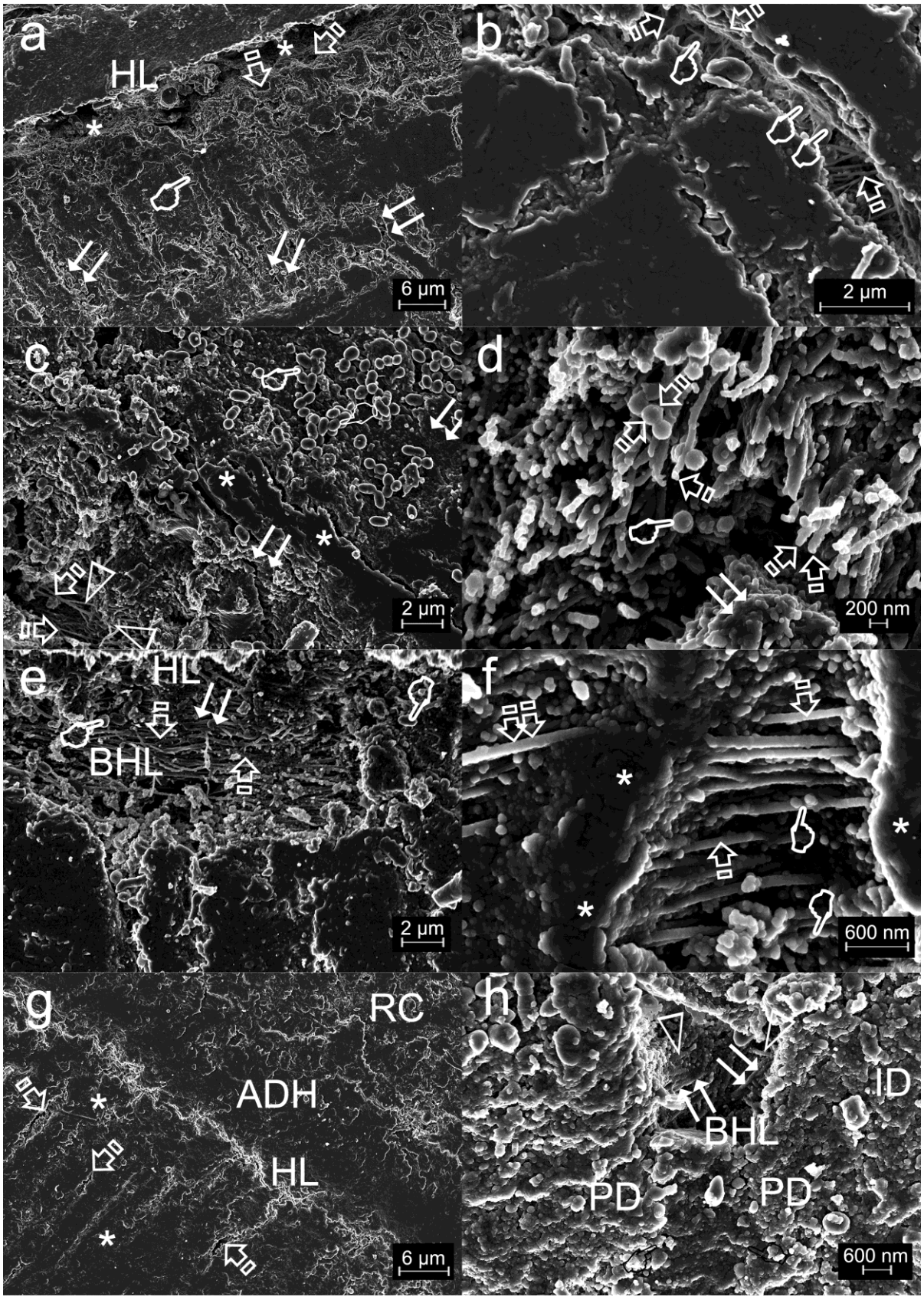
a
HL
6 µm
b
2 µm
c
2 µm
d
200 nm
e
HL
BHL
2 µm
f
600 nm
g
RC
ADH
HL
6 µm
h
ID
BHL
PD
PD
600 nm

Figure 4. Field emission scanning electron microscopy images of the resin-dentin inter-diffusion zone tested after 7 d of storage. **a, b**: Dentin interface bonded with Single Bond adhesive and water/ethanol as pre-treatment. Open (arrows) and filled (pointers) dentinal tubules were observed crossing over the dentin surface. Demineralized collagen fibers (asterisks) below the hybrid layer (HL) and multiple bacteria (double arrows) were discovered in **a**. At a higher magnification (**b**), non-mineralized and resin unprotected collagen fibbers (arrows) were apparent. Collagen fibbers showed reduced diameter. Bacterial anchorage on unprotected collagen was evident in **b** (pointers) [Scale bar: 3 µm (a), 1 µm (b)]. **c, d**: Dentin interface in which undoped-NPs were infiltrated before bonding. Mineral deposits (double arrows), denuded collagen fibers (arrows) and adhesive resin (asterisks) were shown. Collagen fibbers exhibited diameters of about 100 nm, and periodical striations (triangles). A profuse bacterial consortium colonized the infiltrated dentin (pointers), in **c**. Disrupted collagen fibbers showing loose ends which are non mineralized or resin protected were evident in **d** (arrows). Solely few individual (pointers) or associated (faced arrows) NPs appeared onto the degraded dentin surface. Localized mineralization was evident (double arrows) [Scale bar: 1 µm (c), 100 nm (d)]. **e, f**: Dentin interface where Dox-NPs were infiltrated before bonding. A reticular pattern of staggered and demineralized collagen fibrils (arrows) was observed below the HL, crossing over the intertubular dentin at the BHL. Within the resin-dentin interface, a gap detaching the HL from the BHL was formed (double arrows). Minimal amount of bacteria was adverted (pointers) onto the non remineralized dentin, in **e**. At high magnification, staggered and demineralized collagen fibrils (arrows) were observed covering two neighbor demineralized and non resin-infiltrated tubules, which appeared totally empty, in **f**. At peritubular dentin, mineral formed a collar around each tubule lumen observed (asterisks). Mineralized collagen fibers and NPs formed the tubular wall (pointers) [Scale bar: 1 µm (e), 300 nm (f)]. **g, h**: Dentin interface where Zn-NPs were infiltrated before bonding. The resin composite (RC) and the adhesive (ADH) were visible. Thick HL was observed and mineralized collagen fibrils were not noticeable below new mineral deposits. Tubules were scarcely observed (arrows). Mineralization was detected as a dense network of multilayered mineral deposits on the dentin surface (asterisks) and bacterial were hardly encountered, in **g**. Intertubular (ID) and peritubular dentin (PD) appeared entirely remineralized. Tubules were almost totally occluded (pointers). A complete remineralized web of collagen fibbers (double arrows) were discovered at the bottom of the hybrid layer (BHL) in **h**. Fibrils exhibited a width of around 100-200 nm and the typical 67-nm periodicity (triangles). Minimal amount of bacterial colonized the specimens. [Scale bar: 3 µm (g), 300 nm (h), 100 nm (inset)].

Supplementary Material

Title: Polymeric nanoparticles protect the resin-dentin bonded interface from cariogenic biofilm degradation.

Running title: Nanoparticles antidegradation activity at bonded dentin.

Authors:

Manuel Toledano-Osorio[a], Raquel Osorio[a], Fátima S Aguilera[a], Antonio Luis Medina-Castillo[b], Manuel Toledano[a*], Estrella Osorio[a], Sergio Acosta[c], Ruoqiong Chen[d], Conrado Aparicio[e].

Institution:

[a] University of Granada, Faculty of Dentistry, Dental Materials Section.
Colegio Máximo de Cartuja s/n
18071 – Granada - Spain.

[b] University of Granada, NanoMyP. Spin-Off Enterprise.
Edificio BIC-Granada. Av. Innovación 1.
18016 - Armilla, Granada, Spain.

[c] Bioforge lab, CIBER-BBN, Edificio LUCIA, University of Valladolid, Paseo Belen 19, Valladolid 47011, Spain.

[d] Department of Diagnostic and Biological Sciences, School of Dentistry, University of Minnesota, Minneapolis, MN, USA.

[e] MDRCBB-Minnesota Dental Research Center for Biomaterials and Biomechanics, Department of Restorative Sciences, School of Dentistry, University of Minnesota, Minneapolis, MN, USA.

*Corresponding author: Prof. Manuel Toledano.
University of Granada, Faculty of Dentistry
Dental Materials Section
Colegio Máximo de Cartuja s/n
18071 – Granada - Spain.
Tel.: +34-958243788
Fax: +34-958240809
Email: toledano@ugr.es

Figure 1SI.

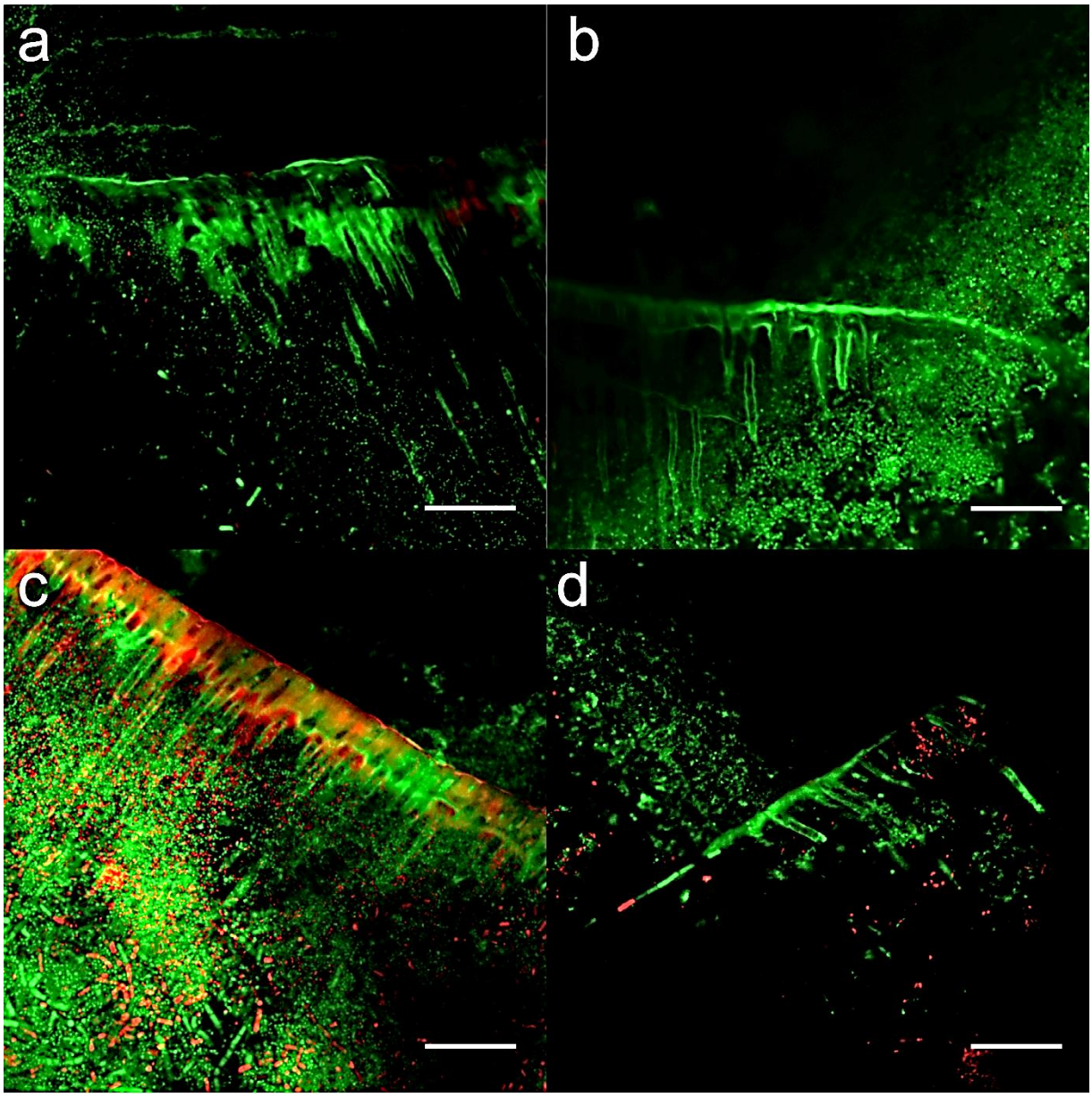

Figure 2SI.

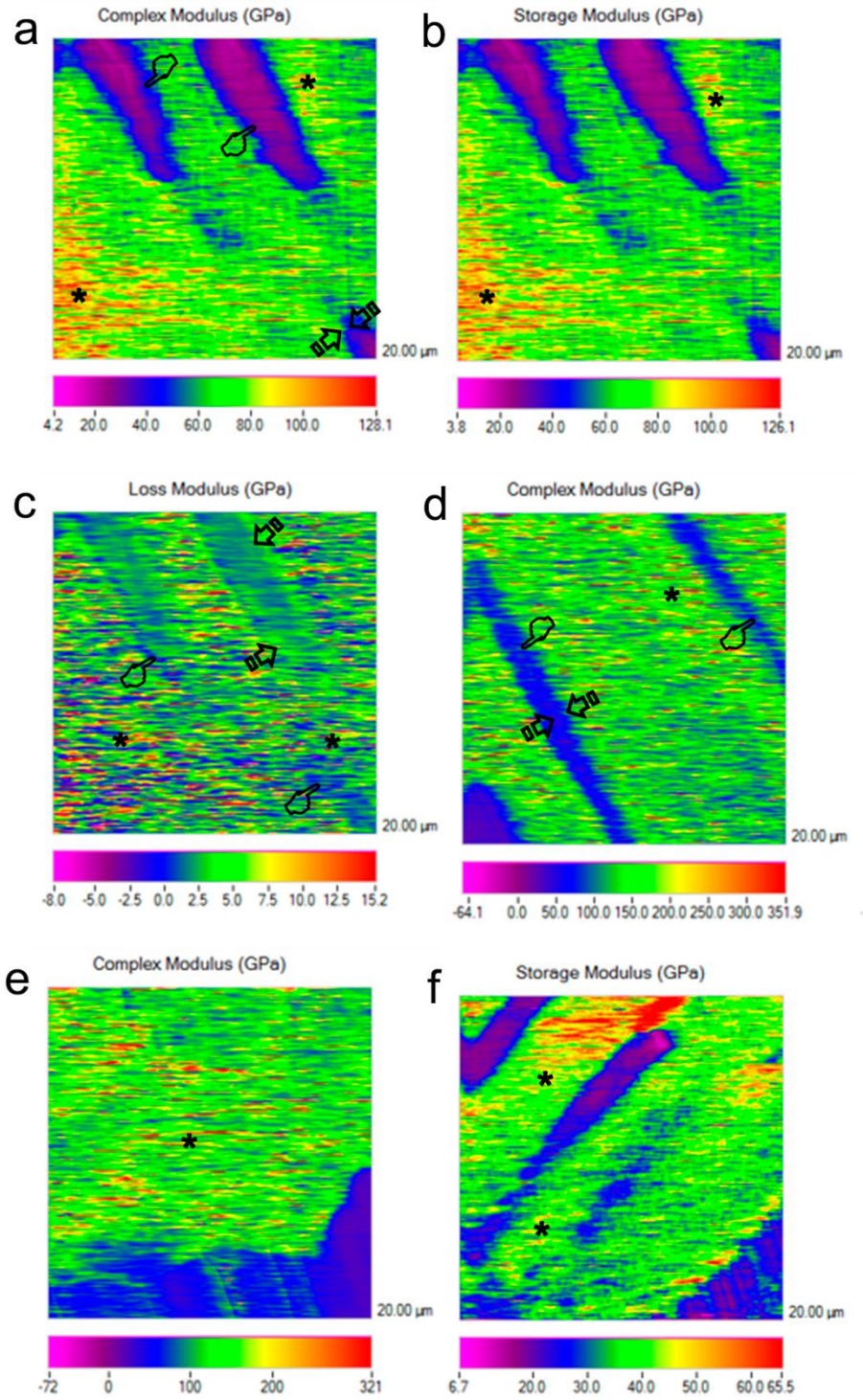
a
Complex Modulus (GPa)
20.00 µm
4.2 20.0 40.0 60.0 80.0 100.0 128.1
b
Storage Modulus (GPa)
20.00 µm
3.8 20.0 40.0 60.0 80.0 100.0 126.1
c
Loss Modulus (GPa)
20.00 µm
-8.0 -5.0 -2.5 0.0 2.5 5.0 7.5 10.0 12.5 15.2
d
Complex Modulus (GPa)
20.00 µm
-64.1 0.0 50.0 100.0 150.0 200.0 250.0 300.0 351.9
e
Complex Modulus (GPa)
20.00 µm
-72 0 100 200 321
f
Storage Modulus (GPa)
20.00 µm
6.7 20.0 30.0 40.0 50.0 60.0 65.5

Figure 2SI. 2D maps (20 x 20 μm) performed at scanning mode by nano-DMA analysis of the complex modulus (*E**), at the resin-dentin interface treated with Zn-NPs, obtained at 7 d (**a**) and 72 h (**e, f**) time points. In the color scheme shown, the red color corresponds to the highest value of the locally measured moduli, likely corresponding to the highest resistance to deformation of the intertubular dentin (asterisks). *E** referred to peritubular dentin appears in blue color (pointers). The pixel data array at the mapping is organized according to *E** distribution that concurs with a clear delimitation between intertubular and peritubular dentin (faced arrows). Scanning mode nano-DMA analysis of the map of the storage modulus (*E'*) at the resin-dentin interface treated with Zn-NPs at 7 d (**b**) and Dox-NPs at 72 h time points (**f**). In the color scheme shown, the red color corresponds to the highest value of the locally *E'* value moduli, potentially associated to the highest ability of the intertubular dentin to storage energy, yellowish-red and yellowish-green in **b** and **f** respectively, at the mappings. 2D scanning mode nano-DMA analysis of the map of the loss modulus (*E''*) at the resin-dentin interface treated with Zn-NPs (**c**). High loss moduli, or viscous behavior values (asterisks), were observed in **c** at intertubular dentin (yellow and red), in contrast with the hybrid layer (blue) (pointers) and the bottom of the hybrid layer (green) (arrows).

Figure 3SI.

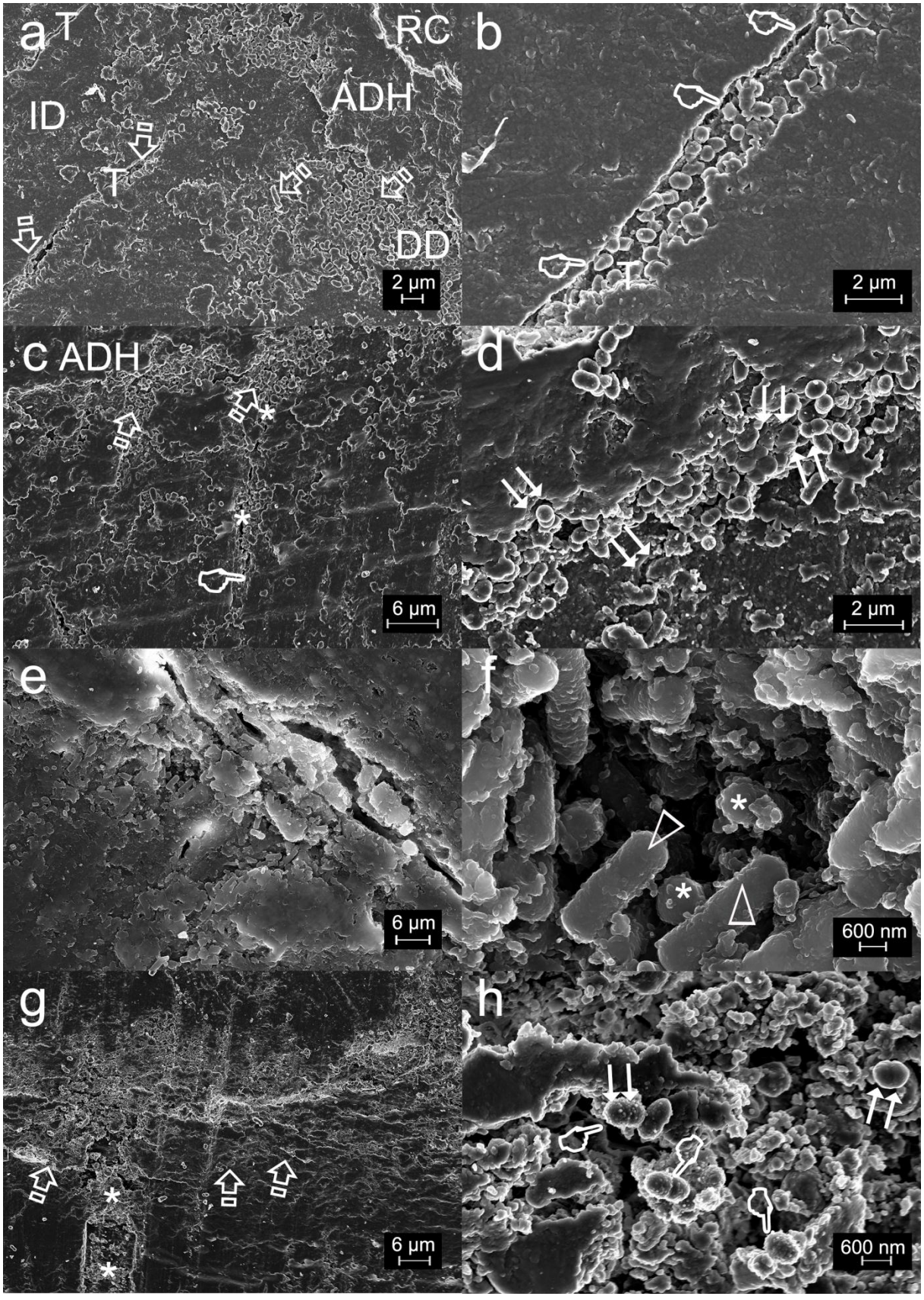
a
T
RC
ADH
ID
T
DD
2 µm
b
T
2 µm
c ADH
6 µm
d
2 µm
e
6 µm
f
600 nm
g
6 µm
h
600 nm

Figure 3SI. Field emission scanning electron microscopy images of the resin-dentin inter-diffusion zone tested after 72 h. **a, b**: Dentin interface bonded with Single Bond (SB) adhesive and water/ethanol as pre-treatment. An adhesive resin (ADH) layer appeared below the resin-composite (RC) bulk, in **a**. Tubules (T) were observed crossing the intertubular dentin (ID) surface. High density of bacteria could be observed beneath the ADH layer and at intratubular dentin (arrows). Demineralized and non-infiltrated dentin (DD) was present, bacteria are mainly attached to this layer of non-resin infiltrated demineralized collagen. At **b:** Demineralized collagen fibers (pointers) and a bacterial consortium filling the dentinal tubule were shown. Bacteria are adhered to demineralized collagen. This bacterial consortium did not appear attached to the rest of the mineralized surfaces [Scale bar: 1 µm (a), 1 µm (b)]. **c, d**: Dentin interface in which undoped-NPs were infiltrated before bonding. The adhesive layer was shown covering an extensive zone of bacterial colonies (arrows) dispersed in local regions of the gap formed beneath the adhesive layer. Bacteria appeared adhered to demineralized collagen inside the tubules or at the bottom of the hybrid layer. At **c:** Some tubules appeared partially mineral-filled (pointers) and bacteria occupied some empty spaces at intratubular dentin (asterisks). At **c**: Non-resin covered collagen was also observed (double arrows). At **d:** The biofilm reflects a dense cell community, where bacteria and uncovered collagen are intimately associated [Scale bar: 3 µm (c), 1 µm (d)]. **e, f**: Dentin interface where Dox-NPs were infiltrated before bonding. Biofilm was difficult to observe, some isolated cells are encountered at the bottom of the hybrid layer, where bacteria and NPs are intimately associated. Demineralized collagen fibbers are shown (double arrows), at **e**. NPs (asterisks) and coco-bacillary bacteria (triangles) predominated, at **f** [Scale bar: 3 µm (e), 300 nm (f)]. **g, h**: Dentin interface in which Zn-NPs were infiltrated before bonding. Bacteria are hardly encountered. Tubular occlusion was observed (asterisks), and demineralized collagen fibers were not patent at the bottom of the hybrid layer (arrows). At higher magnification (**h**): some bacteria and NPs were observed (pointers). Deep changes in cells membranes were induced by Zn-NPs, showing rougher surfaces with different morphologies (double arrows) [Scale bar: 3 µm (g), 300 nm (h)].

Table 1SI. Mean and standard deviation (SD) of storage (E') and loss (E") modulus (GPa) attained at the experimental resin-dentin interfaces.

		Control				Undoped NPs				Dox-NPs				Zn-NPs			
		No biofilm		Biofilm challenge		No biofilm		Biofilm challenge		No biofilm		Biofilm challenge		No biofilm		Biofilm challenge	
		72h	7d	72h	7d	72h	7d	72h	7d	72h	7d	72h	7d	72h	7d	72h	7d
SM(*E'*) (GPa) Mean (SD)	HL	59.78 (12.43) Aa1	63.27 (9.82) Aa1	39.43 (4.37) Aa1	13.13 (0.96) Bb1	42.22 (7.47) Aa1	69.52 (17.03) Aa1	79.47 (18.90) Ba2	20.44 (2.91) Bb2	40.22 (9.68) Aa1	69.70 (12.15) Aa1	43.29 (7.22) Aa1	68.46 (23.43) Aa4	141.59 (46.69) Aa2	145.54 (51.04) Aa2	162.68 (62.53) Aa3	106.81 (24.76) Aa3
	BHL	35.80 (4.61) Aa1	70.73 (6.98) Aa1	24.58 (2.68) Ba1	19.23 (2.16) Ab1	38.71 (6.87) Aa1	60.96 (15.78) Ab1	64.75 (11.01) Ba2	17.28 (2.26) Bb1	20.24 (8.71) Aa1	67.81 (10.38) Ab1	42.78 (9.15) Ba2	78.55 (27.70) Aa3	133.20 (45.47) Aa2	85.06 (19.59) Aa1	137.62 (37.38) Aa2	110.57 (26.58) Aa2
LM(*E"*) (GPa) Mean (SD)	HL	0.60 (4.12) Aa1	1.70 (2.64) Aa1	4.86 (0.86) B1a	0.96 (0.19) Ab1	3.10 (1.76) Aa1	2.28 (4.58) Aa1	2.61 (7.40) Aa1	4.96 (1.08) Aa2	3.95 (1.74) Aa1	4.07 (3.84) Aa1	3.81 (2.03) Aa1	9.63 (7.84) Aa12	-2.28 (21.74) Aa1	11.47 (20.97) Aa1	19.19 (28.80) Ba2	1.93 (7.99) Ab12
	BHL	2.10 (1.19) Aa1	1.71 (2.46) Aa1	5.75 (1.19) Ba1	0.35 (0.26) Ab1	2.56 (1.83) Aa1	-1.79 (4.37) Aa1	2.51 (3.34) Aa1	5.02 (1.56) Aa2	5.15 (1.79) Aa1	4.81 (4.42) Aa1	3.48 (4.99) Aa1	9.15 (9.83) Aa12	-12.19 (31.74) Aa1	3.53 (5.88) Aa1	9.65 (15.84) Aa1	3.07 (15.88) Aa12

Abbreviations: NPs: Nanoparticles; Zn: Zinc; Dox: Doxycycline; SM: Storage modulus; LM: Loss modulus; HL: Hybrid Layer; BHL: Bottom of the Hybrid Layer.

HL and BHL were analyzed independently. Similar capital letters indicate no significant differences between biofilm groups within the same NPs group and time-points ($p<0.01$). Comparisons within the same biofilm and NPs groups are indicated with similar lowercase letters, meaning no significant differences between time-points (72 h and 7 d of storage) ($p<0.01$). Numbers indicate significant differences among NPs groups, within the same biofilm and time-points groups ($p<0.05$).